

Low Mass Neutron Stars and the Equation of State of Dense Matter

J. Carriere * and C. J. Horowitz†

Nuclear Theory Center and Dept. of Physics, Indiana University, Bloomington, IN 47405

J. Piekarewicz ‡

Department of Physics, Florida State University, Tallahassee, FL 32306

(October 24, 2018)

Neutron-star radii provide useful information on the equation of state of neutron rich matter. Particularly interesting is the density dependence of the equation of state (EOS). For example, the softening of the EOS at high density, where the pressure rises slower than anticipated, could signal a transition to an exotic phase. However, extracting the density dependence of the EOS requires measuring the radii of neutron stars for a broad range of masses. A “normal” $1.4M_{\odot}$ (M_{\odot} =solar mass) neutron star has a central density of a few times nuclear-matter saturation density (ρ_0). In contrast, low mass ($\simeq 0.5M_{\odot}$) neutron stars have central densities near ρ_0 so its radius provides information on the EOS at low density. Unfortunately, low-mass stars are rare because they may be hard to form. Instead, a precision measurement of nuclear radii on atomic nuclei may contain similar information. Indeed, we find a strong correlation between the neutron radius of ^{208}Pb and the radius of a $0.5M_{\odot}$ neutron star. Thus, the radius of a $0.5M_{\odot}$ neutron star can be inferred from a measurement of the the neutron radius of ^{208}Pb . Comparing this value to the measured radius of a $\simeq 1.4M_{\odot}$ neutron star should provide the strongest constraint to date on the density dependence of the equation of state.

I. INTRODUCTION

The structure of neutron stars, particularly their masses and radii, depend critically on the equation of state (EOS) of dense matter [1]. New measurements of masses and radii by state-of-the-art observatories should place important constraints on the EOS. Observing a rapid change of the EOS with density could signal a transition to an exotic phase of matter. Possibilities for new high density phases include pion or kaon condensates [2], strange quark matter [3], and/or a color superconductor [4,5]. Measuring neutron-star radii $R(M)$ for a large range of neutron star masses M is attractive as it would allow one to directly deduce the EOS [6], that is, the pressure as a function of the energy density $P(\epsilon)$.

While the masses of various neutron stars are accurately known [7], precise measurements of their radii do not yet exist. Therefore, several groups are devoting considerable effort at measuring neutron-star radii. Often one deduces the surface temperature T_{∞} and the luminosity L of the star from spectral and distance measurements, respectively. Assuming a black-body spectrum, these measurements determine the surface area, and thus the effective radius R_{∞} , of the star from the Stefan-Boltzmann law:

$$L = 4\pi\sigma R_{\infty}^2 T_{\infty}^4 . \quad (1)$$

Opportunities for precision measurements on neutron-star radii include the isolated neutron star RX J185635-3754 [8,9,10] and quiescent neutron stars in globular clusters, such as CXOU 132619.7-472910.8 [11], where distances are accurately known. Moreover, Sanwal and collaborators have recently detected absorption features in

the radio-quiet neutron star 1E 1207.4-5209 [12] that may provide the mass-to-radius ratio of the star through the determination of the gravitational redshift of the spectral lines. These observations are being complemented by studies that aim at constraining the composition of the neutron-star atmosphere [13]. Finally, models of rotational glitches place a lower limit on the radius of the Vela pulsar at $R_{\infty} \gtrsim 12$ km [14].

While a determination of the mass-radius relation $R(M)$ for a variety of neutron stars would uniquely determine the equation of state, unfortunately all accurately determined masses to date fall within a very small range. Indeed, a recent compilation by Thorsett and Chakrabarty of several radio binary pulsars place their masses in the narrow range of $1.25 - 1.44 M_{\odot}$ [7]. Note that several X-ray binaries appear to have larger masses, perhaps because of accretion. These include Cyg X-2 with a mass of $1.8 \pm 0.2M_{\odot}$ [15], Vela X-1 with $1.9 M_{\odot}$ [16], and 4U 1700-37 [17]. If confirmed, they could provide additional information on the high density EOS. However, these mass determinations are not without controversy [18,19]. On the other hand, it may be difficult to form low mass neutron stars from the collapse of heavier Chandrasekhar mass objects. If so, information on the low density EOS may not be directly available from neutron stars. Thus, it is important to make maximum use of any $R(M)$ measurements even if these are available for only a limited range of masses.

Additional information on the low density EOS may be obtained from precision measurements on atomic nuclei. For example, the neutron radius of a heavy nucleus, such as ^{208}Pb , is closely related to the pressure

of neutron rich matter [20]. Indeed, heavy nuclei develop a neutron-rich skin in response to this pressure. The higher the pressure the further the neutrons are pushed out against surface tension, thereby generating a larger neutron radius. However, nuclear properties depend only on the EOS at normal (in the interior) and below (in the surface) nuclear-matter saturation density ($\rho_0 \approx 0.15$ nucleons/fm³). This is in contrast to conventional $1.4 M_\odot$ neutron stars that, with central densities of several times ρ_0 , also depend on the high-density component of the EOS. This is not the case for low mass neutron stars (of about $1/2 M_\odot$). Reaching central densities near ρ_0 , *low mass neutron stars probe the EOS at similar densities as atomic nuclei*. Therefore, one could infer the radius of low mass neutron stars from detailed measurements on atomic nuclei. Having inferred the radii of low mass neutron stars from a nuclear measurement, combined with the measured radius of a $1.4 M_\odot$ star, may enable one to deduce the density dependence of the EOS. (For a recent discussion on the minimum stable mass of a neutron star see Ref. [21].) The parity radius experiment at Jefferson Laboratory [22] aims to measure accurately and model independently the root-mean-square neutron radius (R_n) of ^{208}Pb via parity violating elastic electron scattering [23]. Such an experiment probes neutron densities because the weak vector charge of a neutron is much larger than that of a proton. The goal of the experiment is to measure R_n to a 1% accuracy (within $\approx \pm 0.05$ fm).

The outline of the paper is as follows. In Sec. II we present a relativistic effective field theory formalism to study relationships between the neutron radius of ^{208}Pb and the radii of neutron stars. Uncertainties in these relationships are estimated by considering a wide range of effective field theory parameters, all of them constrained by known nuclear properties. This formalism has been used previously to study correlations between the neutron radius of ^{208}Pb and the properties of the neutron-star crust [24], the radii of $1.4 M_\odot$ neutron stars [25], and the direct URCA cooling of neutron stars [26]. As the radius of low mass neutron stars depends on the solid crust of nonuniform matter, a treatment of the crust is discussed in Sec. III. Our results, presented in Sec. IV, show a strong correlation between the radius of a low mass neutron star and the neutron radius R_n of ^{208}Pb that is essentially model independent. This is because the structure of both objects depend on the EOS at similar densities. In contrast, the radius of a $1.4 M_\odot$ neutron star shows a considerable model dependence. This is because a $1.4 M_\odot$ neutron star is also sensitive to the EOS at higher densities, and the high density EOS is not constrained by nuclear observables. In Sec. V we conclude that properties of low mass neutron stars can be inferred from measuring properties of atomic nuclei. In particular, the radius of a $1/2 M_\odot$ neutron star can be deduced from a measurement of R_n in ^{208}Pb . One will then be able to directly compare this inferred ra-

dius to the measured radius of an $\approx 1.4 M_\odot$ neutron star to gain information on the density dependence of the EOS. Thus, even if a mass-radius measurement for a single ($\approx 1.4 M_\odot$) neutron star is available, one can use the atomic nucleus to gain information on the density dependence of the EOS. This should provide the most precise determination of the density dependence of the EOS to date and should indicate whether a transition to a high density exotic phase of matter is possible or not.

II. FORMALISM

Our starting point is the relativistic effective-field theory of Ref. [27] supplemented with new couplings between the isoscalar and the isovector mesons. This allows us to correlate nuclear observables, such as the neutron radius of ^{208}Pb , with neutron star properties. We will explore uncertainties in these correlations by considering a range of model parameters. The model has been introduced and discussed in detail in several earlier references [24,25,26], yet a brief summary is included here for completeness.

The interacting Lagrangian density is given by [24,27]

$$\begin{aligned} \mathcal{L}_{\text{int}} = & \bar{\psi} \left[g_s \phi - \left(g_v V_\mu + \frac{g_\rho}{2} \boldsymbol{\tau} \cdot \mathbf{b}_\mu + \frac{e}{2} (1 + \tau_3) A_\mu \right) \gamma^\mu \right] \psi \\ & - \frac{\kappa}{3!} (g_s \phi)^3 - \frac{\lambda}{4!} (g_s \phi)^4 + \frac{\zeta}{4!} g_v^4 (V_\mu V^\mu)^2 \\ & + g_\rho^2 \mathbf{b}_\mu \cdot \mathbf{b}^\mu \left[\Lambda_s g_s^2 \phi^2 + \Lambda_v g_v^2 V_\mu V^\mu \right]. \end{aligned} \quad (2)$$

The model contains an isodoublet nucleon field (ψ) interacting via the exchange of two isoscalar mesons, the scalar sigma (ϕ) and the vector omega (V^μ), one isovector meson, the rho (\mathbf{b}^μ), and the photon (A^μ). In addition to meson-nucleon interactions the Lagrangian density includes scalar and vector self-interactions. Omega-meson self-interactions ζ soften the equation of state at high density. Finally, the nonlinear couplings Λ_s and Λ_v are included to modify the density-dependence of the symmetry energy $a_{\text{sym}}(\rho)$ [24,25,26]. We employ Eq. (2) in a mean field approximation where the meson fields are replaced by their ground state expectation values. The couplings constants in Eq. (2) are fit to nuclear matter and finite nuclei properties. All of the parameter sets considered here, namely, NL3 [28], S271 [24], and Z271 [24] reproduce the following properties of symmetric nuclear matter: saturation at a Fermi momentum of $k_F = 1.30$ fm⁻¹ with a binding energy per nucleon of -16.24 MeV and an incompressibility of $K = 271$ MeV. The various parameter sets differ in their effective masses at saturation density, in their ω -meson self interactions (which are included for Z271 and neglected for NL3 and S271) and in the nonlinear couplings Λ_s and Λ_v (see Table I). Note that the NL3 parametrization has been used extensively to reproduce a variety of nuclear properties [28].

The symmetry energy at saturation density is not well constrained experimentally. However, an average of the symmetry energy at saturation density and the surface symmetry energy is constrained by the binding energy of nuclei. Thus, the following prescription has been adopted: the value of the $NN\rho$ coupling constant is adjusted so that all parameter sets have a symmetry energy of 25.67 MeV at $k_F = 1.15 \text{ fm}^{-1}$. This insures accurate binding energies for heavy nuclei, such as ^{208}Pb . Following this prescription the symmetry energy at saturation density is predicted to be 37.3, 36.6, and 36.3 MeV for parameter sets NL3, S271, and Z271, respectively (for $\Lambda_s = \Lambda_v = 0$). Changing Λ_s or Λ_v changes the density dependence of the symmetry energy by changing the effective rho-meson mass. In general increasing either Λ_s or Λ_v causes the symmetry energy to grow more slowly with density.

The neutron radius of ^{208}Pb depends on the density dependence of the symmetry energy. A large pressure for neutron matter pushes neutrons out against surface tension and leads to a large neutron radius. The pressure depends on the derivative of the energy of symmetric matter with respect to density (which is approximately known) and the derivative of the symmetry energy, $da_{\text{sym}}/d\rho$. Thus parameter sets with a large $da_{\text{sym}}/d\rho$ yield a large neutron radius in ^{208}Pb . Note that all parameter sets approximately reproduce the observed proton radius and binding energy of ^{208}Pb . Therefore changing Λ_s or Λ_v allows one to change the density dependence of the symmetry energy $da_{\text{sym}}/d\rho$, while keeping many other properties fixed. Once the model parameters have been fixed, it is a simple matter to calculate the EOS for uniform matter in beta equilibrium, where the chemical potentials of the neutrons μ_n , protons μ_p , electrons μ_e , and muons μ_μ satisfy,

$$\mu_n - \mu_p = \mu_e = \mu_\mu. \quad (3)$$

Note that the high density interior of a neutron star is assumed to be a uniform liquid; possible transitions to a quark- or meson-condensate phase are neglected.

TABLE I. Model parameters used in the calculations. The parameter κ and the scalar mass m_s are given in MeV. The nucleon, rho, and omega masses are kept fixed at $M = 939$, $m_\rho = 763$, and $m_\omega = 783$ MeV, respectively — except in the case of the NL3 model where it is fixed at $m_\omega = 782.5$ MeV.

Model	m_s	g_s^2	g_v^2	κ	λ	ζ
NL3	508.194	104.3871	165.5854	3.8599	-0.0159049	0
S271	505	81.1071	116.7655	6.68344	-0.01580	0
Z271	465	49.4401	70.6689	6.16960	+0.156341	0.06

III. BOUNDARY BETWEEN CRUST AND INTERIOR

Neutron stars are expected to have a solid inner crust of nonuniform neutron-rich matter above a liquid mantle. The phase transition from solid to liquid is thought to be weakly first order and can be found by comparing a detailed model of the nonuniform crust to the liquid (see for example [29]). Yet in practice, model calculations yield very small density discontinuities at the transition. Therefore a good approximation is to search for the density where the uniform liquid first becomes unstable to small amplitude density oscillations (see for example [30]). This method would yield the exact transition density for a second order phase transition.

The stability analysis of the uniform ground state is based on the relativistic random-phase-approximation (RPA) of Ref. [31] for a system of electrons, protons, and neutrons. The approach is generalized here to accommodate the various nonlinear couplings among the meson fields. We start by considering a plane wave density fluctuation of momentum $q = |\mathbf{q}|$ and zero energy $q_0 = 0$. To describe small amplitude particle-hole (or particle-antiparticle) excitations of the fermions we compute the longitudinal polarization matrix that is defined as follows:

$$\Pi_L = \begin{pmatrix} \Pi_{00}^e & 0 & 0 & 0 \\ 0 & \Pi_s^n + \Pi_s^p & \Pi_m^p & \Pi_m^n \\ 0 & \Pi_m^p & \Pi_{00}^p & 0 \\ 0 & \Pi_m^n & 0 & \Pi_{00}^n \end{pmatrix}. \quad (4)$$

Here the one-one entry describes electrons, the two-two entry protons plus neutrons interacting via scalar mesons, the three-three entry protons interacting with vector mesons and the four-four entry neutrons interacting with vector mesons. The individual polarization insertions are given by

$$i\Pi_s(q, q_0) = \int \frac{d^4p}{(2\pi)^4} \text{Tr} \left[G(p)G(p+q) \right], \quad (5a)$$

$$i\Pi_m(q, q_0) = \int \frac{d^4p}{(2\pi)^4} \text{Tr} \left[G(p)\gamma_0 G(p+q) \right], \quad (5b)$$

$$i\Pi_{00}(q, q_0) = \int \frac{d^4p}{(2\pi)^4} \text{Tr} \left[G(p)\gamma_0 G(p+q)\gamma_0 \right], \quad (5c)$$

where Tr indicates a trace over Dirac indices. Note that the fermion Green's function has been defined as

$$G(p) = (\not{p} + M^*) \left(\frac{1}{p^{*2} - M^{*2}} + \frac{i\pi}{E_p^*} \delta(p_0^* - E_p^*) \theta(k_F - |\mathbf{p}|) \right). \quad (6)$$

Here k_F is the Fermi momentum, $M^* = M - g_s\phi_0$ is the nucleon effective mass, $E_p^* = (p^2 + M^{*2})^{1/2}$, and $p_\mu^* = p_\mu - (g_v V_\mu \pm g_\rho b_\mu/2)$ (with the plus sign for protons

and the minus sign for neutrons). Note that in the case of the electrons $M^* = m_e$ and $p_\mu^* = p_\mu$. Explicit analytic formulas for Π_{00} , Π_s , and Π_m in the static limit ($q_0=0$) are given in the appendix.

The lowest order meson propagator D_L^0 is computed in Ref. [31] in the absence of nonlinear meson couplings. It is given by,

$$D_L^0 = \begin{pmatrix} d_g & 0 & -d_g & 0 \\ 0 & -d_s^0 & 0 & 0 \\ -d_g & 0 & d_g + d_v^0 + d_\rho^0 & d_v^0 - d_\rho^0 \\ 0 & 0 & d_v^0 - d_\rho^0 & d_v^0 + d_\rho^0 \end{pmatrix}. \quad (7)$$

Expressions for the photon and for the various meson propagators in the limit of no nonlinear meson couplings are given as follows:

$$d_g = \frac{e^2}{q^2} = \frac{4\pi\alpha}{q^2}, \quad (8a)$$

$$d_s^0 = \frac{g_s^2}{q^2 + m_s^2}, \quad (8b)$$

$$d_v^0 = \frac{g_v^2}{q^2 + m_v^2}, \quad (8c)$$

$$d_\rho^0 = \frac{g_\rho^2/4}{q^2 + m_\rho^2}. \quad (8d)$$

The appearance of a minus sign in the one-three element of D_L^0 relative to the one-one element is because electrons and protons have opposite electric charges.

The addition of nonlinear couplings in the Lagrangian leads to a modification of the meson masses. Effective meson masses are defined in terms of the quadratic fluctuations of the meson fields around their static, mean-field values (the linear fluctuations vanish by virtue of the mean-field equations). That is,

$$m_s^{*2} = -\frac{\partial^2 \mathcal{L}}{\partial \phi_0^2}, \quad m_v^{*2} = +\frac{\partial^2 \mathcal{L}}{\partial V_0^2}, \quad m_\rho^{*2} = +\frac{\partial^2 \mathcal{L}}{\partial b_0^2}. \quad (9)$$

This yields the following expressions for the effective meson masses in terms of the static meson fields and the coupling constants defined in the interacting Lagrangian of Eq. (2):

$$m_s^{*2} = m_s^2 + g_s^2 \left(\kappa \Phi_0 + \frac{\lambda}{2} \Phi_0^2 - 2\Lambda_s B_0^2 \right), \quad (10a)$$

$$m_v^{*2} = m_v^2 + g_v^2 \left(\frac{\zeta}{2} W_0^2 + 2\Lambda_v B_0^2 \right), \quad (10b)$$

$$m_\rho^{*2} = m_\rho^2 + g_\rho^2 (2\Lambda_s \Phi_0^2 + 2\Lambda_v W_0^2). \quad (10c)$$

Note that the following definitions have been introduced: $\Phi_0 \equiv g_s \phi_0$, $W_0 \equiv g_v V_0$, and $B_0 \equiv g_\rho b_0$.

Further, the new couplings between isoscalar and isovector mesons (Λ_s and Λ_v) lead to additional off diagonal terms in the meson propagator. These arise because the quadratic fluctuations around the static solutions generate terms of the form

$$\frac{\partial^2 \mathcal{L}}{\partial \phi_0 \partial b_0} \neq 0 \quad \text{and} \quad \frac{\partial^2 \mathcal{L}}{\partial V_0 \partial b_0} \neq 0. \quad (11)$$

For simplicity we only consider here the following two cases: *i*) ($\Lambda_s \neq 0$ and $\Lambda_v = 0$) or *ii*) ($\Lambda_s = 0$ and $\Lambda_v \neq 0$), and neglect the (slightly) more complicated case in which both coupling constants are different from zero.

For the first case of ($\Lambda_s \neq 0$ and $\Lambda_v = 0$) the new components of the longitudinal meson propagator become

$$d_v = \frac{g_v^2}{q^2 + m_v^{*2}}, \quad (12a)$$

$$d_s = \frac{g_s^2(q^2 + m_\rho^{*2})}{(q^2 + m_s^{*2})(q^2 + m_\rho^{*2}) + (4g_s g_\rho \Lambda_s \Phi_0 B_0)^2}, \quad (12b)$$

$$d_\rho = \frac{(g_\rho^2/4)(q^2 + m_s^{*2})}{(q^2 + m_s^{*2})(q^2 + m_\rho^{*2}) + (4g_s g_\rho \Lambda_s \Phi_0 B_0)^2}, \quad (12c)$$

$$d_{s\rho} = \frac{2g_s^2 g_\rho^2 \Lambda_s \Phi_0 B_0}{(q^2 + m_s^{*2})(q^2 + m_\rho^{*2}) + (4g_s g_\rho \Lambda_s \Phi_0 B_0)^2}. \quad (12d)$$

With these changes the modified longitudinal meson propagator now reads,

$$D_L = \begin{pmatrix} d_g & 0 & -d_g & 0 \\ 0 & -d_s & d_{s\rho} & -d_{s\rho} \\ -d_g & d_{s\rho} & d_g + d_v + d_\rho & d_v - d_\rho \\ 0 & -d_{s\rho} & d_v - d_\rho & d_v + d_\rho \end{pmatrix}. \quad (13)$$

Alternatively, for the case of ($\Lambda_s = 0$ and $\Lambda_v \neq 0$) we obtain,

$$d_s = \frac{g_s^2}{q^2 + m_s^{*2}}, \quad (14a)$$

$$d_v = \frac{g_v^2(q^2 + m_\rho^{*2})}{(q^2 + m_v^{*2})(q^2 + m_\rho^{*2}) - (4g_v g_\rho \Lambda_v W_0 B_0)^2}, \quad (14b)$$

$$d_\rho = \frac{(g_\rho^2/4)(q^2 + m_v^{*2})}{(q^2 + m_v^{*2})(q^2 + m_\rho^{*2}) - (4g_v g_\rho \Lambda_v W_0 B_0)^2}, \quad (14c)$$

$$d_{v\rho} = \frac{-2g_v^2 g_\rho^2 \Lambda_v W_0 B_0}{(q^2 + m_v^{*2})(q^2 + m_\rho^{*2}) - (4g_v g_\rho \Lambda_v W_0 B_0)^2}. \quad (14d)$$

With these changes the modified longitudinal meson propagator now reads,

$$D_L = \begin{pmatrix} d_g & 0 & -d_g & 0 \\ 0 & -d_s & 0 & 0 \\ -d_g & 0 & d_g + d_v + d_\rho + 2d_{v\rho} & d_v - d_\rho \\ 0 & 0 & d_v - d_\rho & d_v + d_\rho - 2d_{v\rho} \end{pmatrix}. \quad (15)$$

The uniform system becomes unstable to small amplitude density fluctuations of momentum transfer q when the following condition is satisfied:

$$\det[1 - D_L(q)\Pi_L(q, q_0=0)] \leq 0. \quad (16)$$

We estimate the transition density (ρ_c) between the inner crust and the liquid interior as the largest density for which Eq. (16) has a solution. Our results for ρ_c are listed in Tables II-V and also shown in Fig. 1. We find a strong correlation between the neutron skin of ^{208}Pb and

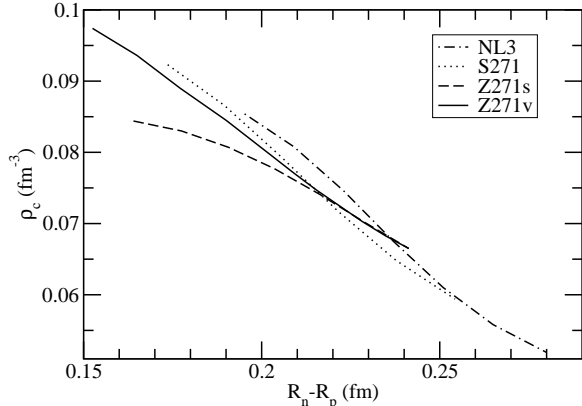


FIG. 1. The transition density ρ_c at which uniform matter becomes unstable to density oscillations as a function of the neutron skin in ^{208}Pb . The solid line is for the Z271 parameter set with $\Lambda_v \neq 0$ while the dashed curve uses Z271 with $\Lambda_s \neq 0$. The dotted curve is for the S271 set and the dot-dashed curve for NL3, both of these with $\Lambda_v \neq 0$.

At the lower densities of the inner crust the system is nonuniform and may have a very complex structure that may include spherical, cylindrical, and plate-like nuclei, bubbles, rods, plates, *etc.* [32,33]. At present we do not have microscopic calculations of these structures in our models. Therefore we adopt a simple interpolation formula to estimate the equation of state in the inner crust. That is, we assume a polytropic form for the EOS in which the pressure is approximately given by [14],

$$P(\epsilon) = A + B\epsilon^{4/3}, \quad (17)$$

where ϵ is the mass-energy density. The two constants A and B in Eq. (17) are chosen so that the pressure is continuous at the boundary between the inner crust and the liquid interior (determined from the RPA analysis) and at the boundary between the inner and the outer crusts. For the low density outer crust we assume the EOS of Baym, Pethick, and Sutherland (BPS) [34] up to a baryon density of $\rho_{\text{outer}} = 2.57 \times 10^{-4} \text{ fm}^{-3}$ which corresponds to an energy density of $\epsilon_{\text{outer}} = 4.30 \times 10^{11} \text{ g/cm}^3$ (or 0.24 MeV/fm^3) and a pressure of $P_{\text{outer}} = 4.87 \times 10^{-4} \text{ MeV/fm}^3$. Thus the two constants A and B of Eq. (17) are adjusted to reproduce P_{outer} at ϵ_{outer} and the pressure of the uniform liquid, calculated within the relativistic mean-field (RMF) approach, at ϵ_c which is the energy density corresponding to ρ_c . That is,

$$P(\epsilon) = \begin{cases} P_{\text{BPS}}(\epsilon), & \text{for } \epsilon_{\text{min}} \leq \epsilon \leq \epsilon_{\text{outer}}; \\ A + B\epsilon^{4/3}, & \text{for } \epsilon_{\text{outer}} < \epsilon \leq \epsilon_c; \\ P_{\text{RMF}}(\epsilon), & \text{for } \epsilon_c < \epsilon. \end{cases} \quad (18)$$

Note that $\epsilon_{\text{min}} = 5.86 \times 10^{-9} \text{ MeV/fm}^3$ is the minimum value of the energy density included in the equation of state. This value corresponds to a minimum pressure of $P_{\text{min}} = 6.08 \times 10^{-15} \text{ MeV/fm}^3$, which is the value at which we stop integrating the Tolman-Oppenheimer-Volkoff equations. That is, the radius R of a neutron star (see Sec. IV) is defined by the expression $P(R) = P_{\text{min}}$. For the relativistic mean field interaction (TM1) of Ref. [35], the relatively simple procedure presented here is a good approximation to the more complicated explicit calculation of the EOS in the inner crust [36].

IV. RESULTS

Figures 2-5 and Tables II-V show the radii of neutron stars of mass $1/3, 1/2, 3/4$ and $1.4 M_{\odot}$ as a function of the neutron skin ($R_n - R_p$) of ^{208}Pb . One might expect a strong correlation between the radius of a neutron star and the neutron radius of ^{208}Pb , as the same pressure of neutron rich matter that pushes neutrons out against surface tension in ^{208}Pb pushes neutrons out against gravity in a neutron star [25]. However, the central density of a $1.4 M_{\odot}$ neutron star is a few times larger than normal nuclear-matter saturation density ρ_0 . Thus, $R(1.4 M_{\odot})$ depends on the EOS at low and high densities while R_n only depends on the EOS for $\rho \leq \rho_0$. Softening the EOS (*i.e.*, decreasing the pressure) at high densities will decrease $R(1.4 M_{\odot})$ without changing R_n . Hence, while Fig. 5 shows a definite correlation— $R(1.4 M_{\odot})$ grows with increasing $R_n - R_p$ —there is a strong model dependence.

In contrast, the central density of a $\frac{1}{2} M_{\odot}$ star is of the order of ρ_0 , so $R(\frac{1}{2} M_{\odot})$ and R_n depend on the EOS over a comparable density range. As a result, we find a strong correlation and weak model dependence in Fig. 3. For example, if $R_n - R_p$ in ^{208}Pb is relatively large, *e.g.*, $R_n - R_p \approx 0.25 \text{ fm}$, then $R(\frac{1}{2} M_{\odot}) \approx 16 \text{ km}$. Alternatively, if $R_n - R_p \approx 0.15 \text{ fm}$, then $R(\frac{1}{2} M_{\odot}) \lesssim 13 \text{ km}$. This is an important result. It suggests that even if observations of low mass neutron stars are not feasible, one could still infer their radii from a single nuclear measurement. Note that the results for a $\frac{3}{4} M_{\odot}$ neutron star (Fig. 4) follow a similar trend.

We conclude this section with a comment on $\frac{1}{3} M_{\odot}$ neutron stars. Parameter sets that generate very large values for $R_n - R_p$ have large pressures near ρ_0 . This implies that the energy of neutron rich matter rises rapidly with density. In turn, this leads (because all parameter sets are constrained to have the same symmetry energy at $\rho = 0.1 \text{ fm}^{-3}$) to lower energies and *lower pressures* at very low density as compared with parameter sets with smaller values for $R_n - R_p$. This low-density region is important for low mass neutron stars and could explain why $R(\frac{1}{3} M_{\odot})$ in Fig. 2 actually decreases with increasing neutron skin for $R_n - R_p \gtrsim 0.23 \text{ fm}$.

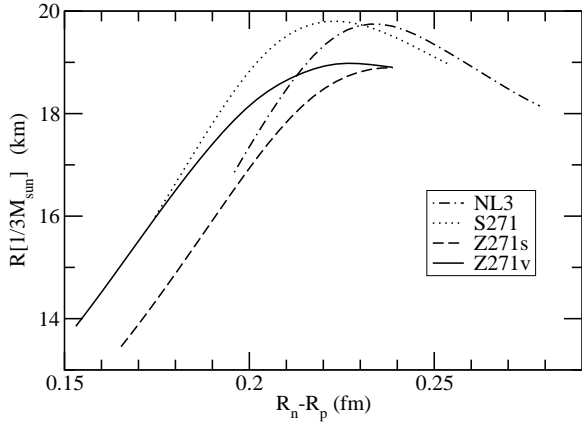


FIG. 2. Radius of a neutron star of mass $1/3 M_\odot$ as a function of the neutron skin in ^{208}Pb . The solid line is for the Z271 parameter set with $\Lambda_v \neq 0$ while the dashed curve uses Z271 with $\Lambda_s \neq 0$. The dotted curve is for the S271 set and the dot-dashed curve for NL3, both of these with $\Lambda_v \neq 0$.

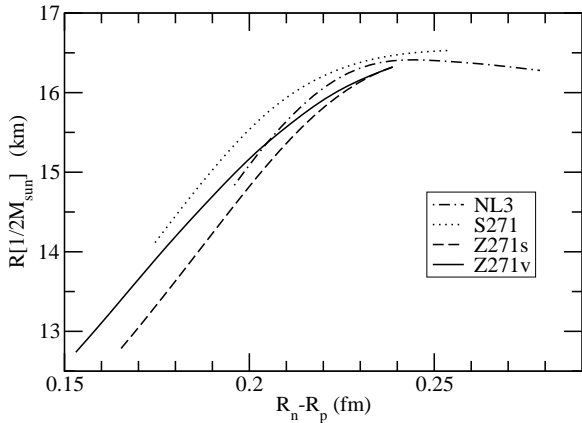


FIG. 3. Radius of a neutron star of mass $1/2 M_\odot$ as a function of the neutron skin in ^{208}Pb . The solid line is for the Z271 parameter set with $\Lambda_v \neq 0$ while the dashed curve uses Z271 with $\Lambda_s \neq 0$. The dotted curve is for the S271 set and the dot-dashed curve for NL3, both of these with $\Lambda_v \neq 0$.

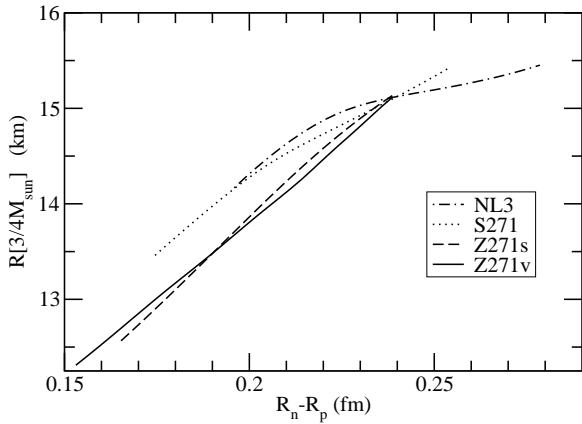


FIG. 4. Radius of a neutron star of mass $3/4 M_\odot$ as a function of the neutron skin in ^{208}Pb . The solid line is for the Z271 parameter set with $\Lambda_v \neq 0$ while the dashed curve uses Z271 with $\Lambda_s \neq 0$. The dotted curve is for the S271 set and the dot-dashed curve for NL3, both of these with $\Lambda_v \neq 0$.

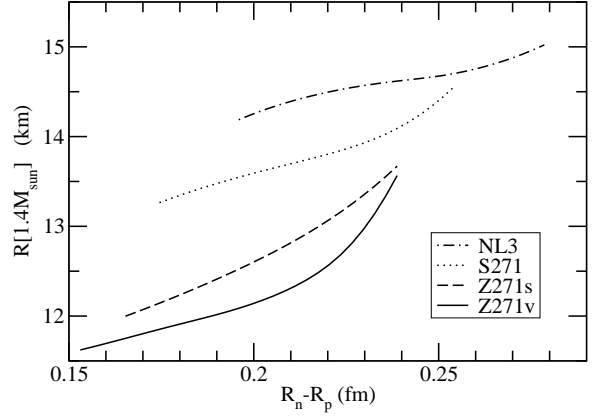


FIG. 5. Radius of a neutron star of mass $1.4 M_\odot$ as a function of the neutron skin in ^{208}Pb . The solid line is for the Z271 parameter set with $\Lambda_v \neq 0$ while the dashed curve uses Z271 with $\Lambda_s \neq 0$. The dotted curve is for the S271 set and the dot-dashed curve for NL3, both of these with $\Lambda_v \neq 0$.

TABLE II. Results for the NL3 parameter set with $\Lambda_s = 0$. The $NN\rho$ coupling constant g_ρ^2 and the neutron minus proton root mean square radius for ^{208}Pb (in fm) are given along with the radii of 1/3, 1/2, 3/4 and 1.4 M_\odot neutron stars in km. Finally, the transition density ρ_c between the inner crust and liquid interior is given in fm^{-3} .

Λ_v	g_ρ^2	$R_n - R_p(^{208}\text{Pb})$	$R(\frac{1}{3}M_\odot)$	$R(\frac{1}{2}M_\odot)$	$R(\frac{3}{4}M_\odot)$	$R(1.4M_\odot)$	ρ_c
0.030	127.0	0.1952	16.766	14.789	14.142	14.175	0.0854
0.025	115.6	0.209	18.37	15.59	14.60	14.38	0.0808
0.020	106.0	0.223	19.49	16.15	14.93	14.52	0.0746
0.015	97.9	0.237	19.73	16.39	15.10	14.61	0.0675
0.010	90.9	0.251	19.31	16.40	15.20	14.68	0.0610
0.005	84.9	0.265	18.70	16.35	15.31	14.81	0.0558
0.000	79.6	0.280	18.10	16.27	15.47	15.05	0.0519

TABLE III. Results for the S271 parameter set with $\Lambda_s = 0$. The $NN\rho$ coupling constant g_ρ^2 and the neutron minus proton root mean square radius for ^{208}Pb (in fm) are given along with the radii of 1/3, 1/2, 3/4 and 1.4 M_\odot neutron stars in km. Finally, the transition density ρ_c between the inner crust and liquid interior is given in fm^{-3} .

Λ_v	g_ρ^2	$R_n - R_p(^{208}\text{Pb})$	$R(\frac{1}{3}M_\odot)$	$R(\frac{1}{2}M_\odot)$	$R(\frac{3}{4}M_\odot)$	$R(1.4M_\odot)$	ρ_c
0.05	127.8389	0.1736	15.88	14.06	13.43	13.25	0.0923
0.04	116.2950	0.1895	17.75	15.00	13.96	13.47	0.0866
0.03	106.6635	0.2054	19.25	15.77	14.42	13.65	0.0794
0.02	98.5051	0.2215	19.80	16.24	14.76	13.82	0.0717
0.01	91.5061	0.2378	19.54	16.46	15.08	14.07	0.0648
0.00	85.4357	0.2543	18.95	16.53	15.43	14.56	0.0594

TABLE IV. Results for the Z271 parameter set with $\Lambda_s = 0$. The $NN\rho$ coupling constant g_ρ^2 and the neutron minus proton root mean square radius for ^{208}Pb (in fm) are given along with the radii of 1/3, 1/2, 3/4 and 1.4 M_\odot neutron stars in km. Finally, the transition density ρ_c between the inner crust and liquid interior is given in fm^{-3} .

Λ_v	g_ρ^2	$R_n - R_p(^{208}\text{Pb})$	$R(\frac{1}{3}M_\odot)$	$R(\frac{1}{2}M_\odot)$	$R(\frac{3}{4}M_\odot)$	$R(1.4M_\odot)$	ρ_c
0.14	139.3368	0.1525	13.799	12.709	12.293	11.616	0.0974
0.12	129.2795	0.1650	15.012	13.379	12.688	11.748	0.0936
0.10	119.5245	0.1771	16.219	14.039	13.080	11.880	0.0890
0.08	112.9710	0.1900	17.405	14.696	13.481	12.016	0.0845
0.06	106.2682	0.2026	18.31	15.28	13.89	12.18	0.0796
0.05	103.2065	0.2090	18.61	15.53	14.09	12.29	0.0771
0.04	100.3162	0.2154	18.82	15.76	14.30	12.43	0.0747
0.03	97.5834	0.2218	18.95	15.96	14.53	12.62	0.0725
0.02	94.9956	0.2282	18.98	16.12	14.75	12.89	0.0703
0.01	92.5415	0.2347	18.94	16.25	14.98	13.27	0.0683
0.00	90.2110	0.2413	18.88	16.36	15.20	13.77	0.0665

TABLE V. Results for the Z271 parameter set with $\Lambda_v=0$. The $NN\rho$ coupling constant g_ρ^2 and the neutron minus proton root mean square radius for ^{208}Pb (in fm) are given along with the radii of 1/3, 1/2, 3/4 and 1.4 M_\odot neutron stars in km. Finally, the transition density ρ_c between the inner crust and liquid interior is given in fm^{-3} .

Λ_s	g_ρ^2	$R_n - R_p(^{208}\text{Pb})$	$R(\frac{1}{3}M_\odot)$	$R(\frac{1}{2}M_\odot)$	$R(\frac{3}{4}M_\odot)$	$R(1.4M_\odot)$	ρ_c
0.06	146.6988	0.1640	13.34	12.71	12.52	11.98	0.0844
0.05	132.8358	0.1775	14.63	13.48	13.01	12.19	0.0830
0.04	121.3666	0.1907	15.99	14.27	13.51	12.42	0.0807
0.03	111.7205	0.2036	17.28	15.02	14.00	12.68	0.0777
0.02	103.4949	0.2163	18.27	15.66	14.46	12.97	0.0741
0.01	96.3974	0.2288	18.79	16.10	14.86	13.32	0.0702
0.00	90.2110	0.2413	18.88	16.36	15.20	13.77	0.0665

V. DISCUSSION AND CONCLUSIONS

A number of relativistic effective field theory parameter sets have been used to study correlations between the radii of neutron stars and the neutron radius R_n of ^{208}Pb . An RPA stability analysis was employed to find the transition density between the nonuniform inner crust and the uniform liquid interior. For the nonuniform outer crust we invoked the EOS of Baym, Pethick, and Sutherland [34]. Then, a simple polytropic formula for the EOS, approximately valid for most of the crust [14], was used to interpolate between the outer crust and the liquid interior. This simple, yet fairly accurate, procedure allows us to study the EOS for a variety of parameter sets that predict a wide range of values for the neutron radius of ^{208}Pb .

For a “normal” $1.4M_\odot$ neutron star we find central densities of several times normal nuclear matter saturation density ($\rho_0 \approx 0.15 \text{ fm}^{-3}$). Because the neutron radius of ^{208}Pb does not constrain the high-density component of the EOS, we find a strong model dependence between the radius of a $1.4M_\odot$ neutron star and R_n . In contrast, the central density of a low mass neutron star is close to ρ_0 . Therefore properties of the low mass star are sensitive to the EOS over the same density range as R_n . As a result, we find a strong correlation and a weak model dependence between the radius of a $0.5M_\odot$ neutron star and R_n (see Fig. 3). Thus, it should be possible to infer some properties of low mass neutron stars from detailed measurements in atomic nuclei.

Understanding the density dependence of the equation of state is particularly interesting. A softening of the EOS at high density (where the pressure rises slower than expected) could signal the transition to an exotic phase, such as pion/kaon condensates, strange quark matter, and/or a color superconductor. Yet obtaining definitive results on the density dependence of the EOS may require measuring the radius of neutron stars for a broad range of masses. This may be difficult as most compilations to date find neutron star masses in the very narrow range of $1.25 - 1.44 M_\odot$ [7]. Further, important ambiguities will

remain if the radius of a $1.4M_\odot$ neutron star proves to be moderately small. Would a small radius be an indication that the EOS is relatively soft at all densities and there is no phase transition, or is the EOS stiff at low density and undergoes an abrupt softening at high density from a phase transition?

Therefore, it is important to also make measurements that are exclusively sensitive to the low density EOS. One obvious possibility is the radius of a low mass ($\approx 0.5M_\odot$) neutron star as its central density, close to ρ_0 , is much smaller than that of a $1.4M_\odot$ star. However such low mass stars may be very rare because they are hard to form. Notably, the neutron radius of a heavy nucleus, such as ^{208}Pb , contains similar information. Indeed, we find a strong correlation and a weak model dependence between the neutron radius of ^{208}Pb and the radius of a $0.5M_\odot$ neutron star. This allows one to use nuclear information to infer the radius of a low mass neutron star. Hence, comparing this inferred radius to the measured radius of a $\approx 1.4M_\odot$ neutron star, should provide the most complete information to date on the density dependence of the equation of state.

This work was supported in part by DOE grants DE-FG02-87ER40365 and DE-FG05-92ER40750.

VI. APPENDIX

The polarizations are defined in Eqs. (5a,5b,5c) and describe particle-hole or particle antiparticle excitations. In the static limit (energy transfer $q_0=0$) the scalar polarization for momentum transfer q is given by

$$\Pi_s(q, 0) = \frac{1}{2\pi^2} \left\{ k_F E_F - \left(3M^{*2} + \frac{q^2}{2} \right) \ln \frac{k_F + E_F}{M^*} + \frac{2E_F E^2}{q} \ln \left| \frac{2k_F - q}{2k_F + q} \right| - \frac{2E^3}{q} \ln \left| \frac{qE_F - 2k_F E}{qE_F + 2k_F E} \right| \right\}, \quad (19)$$

with Fermi momentum k_F , nucleon effective mass M^* , $E_F = (k_F^2 + M^{*2})^{1/2}$, and $E = (q^2/4 + M^{*2})^{1/2}$. Likewise, the longitudinal polarization is given by

$$\Pi_{00}(q, 0) = -\frac{1}{\pi^2} \left\{ \frac{2}{3} k_F E_F - \frac{q^2}{6} \ln \frac{k_F + E_F}{M^*} - \frac{E_F}{3q} (M^{*2} + k_F^2 - \frac{3}{4} q^2) \ln \left| \frac{2k_F - q}{2k_F + q} \right| + \frac{E}{3q} (M^{*2} - \frac{q^2}{2}) \ln \left| \frac{qE_F - 2k_F E}{qE_F + 2k_F E} \right| \right\}, \quad (20)$$

while the mixed scalar-vector polarization becomes

$$\Pi_m(q, 0) = \frac{M^*}{2\pi^2} \left\{ k_F - \left(\frac{k_F^2}{q} - \frac{q}{4} \right) \ln \left| \frac{2k_F - q}{2k_F + q} \right| \right\}. \quad (21)$$

-
- [1] J. M. Lattimer and M. Prakash, ApJ. **550** (2001) 426.
 - [2] J.A. Pons, J.A. Miralles, M. Prakash, J.M. Lattimer, ApJ. **553**, (2001) 382.
 - [3] P. Jaikumar and M. Prakash, astro-ph/0105225. M. Prakash, Nucl. Phys. **A698**, (2002) 440.
 - [4] H. Heiselberg, *Proceedings of the Conference on Compact Stars in the QCD Phase Diagram*, (2001) 3; astro-ph/0201465.
 - [5] M. Alford, *Proceedings of the Conference on Compact Stars in the QCD Phase Diagram*, (2001) 137; hep-ph/0110150.
 - [6] L. Lindblom, ApJ. **398**, (1992) 569.
 - [7] S. E. Thorsett and D. Chakrabarty, ApJ. **512** (1999) 288.
 - [8] F. M. Walter and J. Lattimer, astro-ph/0204199.
 - [9] J.J. Drake et al., ApJ in press, astro-ph/0204159.
 - [10] J. A. Pons, F. M. Walter, J. M. Lattimer, M. Prakash, R. Neuhauser, and P. An, ApJ. **564** (2002) 981.
 - [11] E. F. Brown, L. Bildsten, and R. E. Rutledge, ApJ. **504** (1998) L95; R.E. Rutledge, L. Bildsten, E.F. Brown, G.G. Pavlov, and V.E. Zavlin, astro-ph/0105405.
 - [12] D. Sanwal, G. G. Pavlov, V. E. Zavlin, and M. A. Teter, ApJ. **574** (2002) L61.
 - [13] C. J. Hailey and K. Mori, astro-ph/0207590.
 - [14] B. Link, R. I. Epstein, and J. M. Lattimer, Phys Rev. Lett. **83** (1999) 3362.
 - [15] J. A. Orosz and E. Kuulkers, MNRAS **305** (1999) 132.
 - [16] J.H. van Kerkwijk, J van Paradijs, and E.J. Zuiderwijk, A&A **303** 497.
 - [17] S.R. Heap and M.F. Corcoran, ApJ. **387** (1992) 340.
 - [18] D. Stickland, C. Lloyd, and A. Radzuin-Woodham, MNRAS **286** (1997) L21.
 - [19] G.E. Brown, J.C. Weingartner, and R.A.M.J. Wijers, ApJ. **463** (1996) 297.
 - [20] B. Alex Brown, Phys. Rev. Lett. **85** (2000) 5296.
 - [21] P. Haensel, J. L. Zdunik, and F. Douchin, astro-ph/0201434.
 - [22] Jefferson Laboratory Experiment E-00-003, Spokespersons R. Michaels, P. A. Souder and G. M. Urciuoli.
 - [23] C. J. Horowitz, S. J. Pollock, P. A. Souder and R. Michaels, Phys. Rev. C **63**, 025501 (2001).
 - [24] C.J. Horowitz and J. Piekarewicz, Phys. Rev. Lett. **86**, (2001) 5647.
 - [25] C.J. Horowitz and J. Piekarewicz, Phys. Rev. C **64** (2001) 062802.
 - [26] C.J. Horowitz and J. Piekarewicz, nucl-th/0207067.
 - [27] H. Müller and B. D. Serot, Nucl. Phys. **A606**, 508 (1996).
 - [28] G. A. Lalazissis, J. König and P. Ring, Phys. Rev. C **55** (1997) 540.
 - [29] F. Douchin and P. Haensel, astro-ph/0111092.
 - [30] F. Douchin and P. Haensel, PLB **485** (2000) 107.
 - [31] C.J. Horowitz and K. Wehrberger, NP **A531** (1991) 665.
 - [32] C.P. Lorenz, D.G. Ravenhall, and C.J. Pethick, Phys. Rev. Lett. **70** (1993) 379.
 - [33] K. Oyamatsu, Nucl. Phys. **A561**, (1993) 431.
 - [34] G. Baym, C. Pethick, and P. Sutherland, ApJ. **170** (1971) 299.
 - [35] Y. Sugahara and H. Toki, NP **A579** (1994) 557.
 - [36] H. Shen, H. Toki, K. Oyamatsu, and K. Sumiyoshi, NP **A637** (1998) 435.